J Mater Sci: Mater Med (2010) 21:2057–2066
DOI 10.1007/s10856-010-4079-4

Synthesis, extrusion and rheological behaviour of PU/HA composites for biomedical applications

H. B. Machado · Rui N. Correia · J. A. Covas

Received: 24 November 2008 / Accepted: 1 April 2010 / Published online: 20 April 2010

Abstract Biostable polyurethane/hydroxyapatite (PU/HA) composites with potential application as bone replacement materials were synthesized in bulk and processed in a screw extruder. The polyurethanes (PU) were prepared by reacting an aliphatic diisocyanate, 4-methylene-bis-diisocyanate (MDI), with poly-(ε-caprolactone) (PCL) diols and polytetramethylene oxide (PTMO) of different molecular weights, extended with 1, 4-butanediol (BDO). Glass-transition temperatures were measured by differential *scanning* calorimetry (DSC). The specific PU groups were assessed by total reflectance-Fourier transform infrared spectroscopy (ATR-FTIR). The effects of polymer chemistry and filler content on the rheological behaviour were studied by oscillatory rheometry. Polymers with larger chain lengths showed higher viscosity and, for identical chain lengths, polyether urethanes seem to have higher viscosities than polyester based urethanes. A lubricating effect was found for composites containing 50% weight of filler, whereas at higher filler contents a solid-like behaviour was measured. Polymer chemistry seems to be affected by ageing but not so by the presence of filler. Ageing is characterized by a decrease in the concentration of hydrogen bonds involving between urethane linkages.

H. B. Machado (✉) · R. N. Correia
Department of Ceramic Engineering, Univ. Aveiro,
3810-193 Aveiro, Portugal
e-mail: hmachado@cv.ua.pt

J. A. Covas
Department of Polymer Engineering, IPC/I3 N, Univ. Minho,
4800-058 Azurém, Portugal

1 Introduction

Over the last decade, many efforts have been made towards the development of new bone replacement materials. Among these, hydroxyapatite/polymer composites have attracted much attention, as they may exhibit osteoconductivity [1–5]. However, bioceramics are generally brittle and, consequently, inadequate for load-bearing applications other than those involving resistance to pure compression.

Current polymer compounding technology makes it possible to produce highly filled polymers of excellent quality, thus enabling the manufacture of bioactive, high performing ceramic/polymer composites [6]. PU has proven to be biocompatible and is widely used in medical devices, e.g., in artificial ventricular assist devices, total heart diaphragms, heart valves and vascular grafts [7]. Bioabsorbable PU's have been synthesized, but biodegradation may occur at rates much slower than those desirable in practice [8]. Moreover, these polymers invariably produce toxic by-products such as 4,4 mehtylenedianiline (MDA), which pose severe limitations to their use in vivo.

The successful use of PU's in medical applications is due to their straightforward synthesis and the possibility of introducing functional groups into the polymeric chain, which may lead to the improvement of various properties [9]. Hard and soft segments alternate in their structure. The former are composed of alternating diisocyanate and chain extender molecules (i.e. diol or diamine), while the soft segments are linear long chain diols. Phase separation occurs in these polymers because of incompatibility between hard and soft segments, which aggregate into microdomains and produce a structure composed of glassy and rubbery domains. The hard domains acquire rigidity via crosslinking and confer some reinforcement of the soft segments [10].

These materials need to be stabilized against oxidation and hydrolysis for long term use. Previous studies focused on biodegradation mechanisms using accelerated in vitro tests that mimic in vivo biodegradation showed that poly (ester-urethanes) easily undergo hydrolytic degradation. Poly (ether-urethanes) are more stable regarding hydrolysis, but they are sensitive to oxidation and crosslinking of ether soft segments, the latter being the primary mechanisms of chemical degradation [11–14].

To the authors' knowledge, there are few reports in the open literature concerning the use PU/HA composites for medical use prepared by extrusion. However, in applications mimicking bone composition and entailing the presence of high volume percentages of bioactive HA, PU is an attractive matrix because of its biocompatibility, low rigidity and melt processability, providing the possibility of mass production of implants at reasonable costs [15]. The present study reports the results of experiments involving the synthesis of different PU's, the preparation of PU/HA composites by extrusion, and their characterization. The matrix and hard segment content were varied as well as the percentage of HA, since these parameters are expected to influence degradation, mechanical properties and bioactivity. Because polymer antioxidants sacrifice biocompatibility, an oxygen radical scavenger (butylated hydroxyanisole, BHA) was used instead. It is soluble in PU, acts as an inhibitor of peroxidation and its cytotoxicity is well documented [16–21].

2 Materials and methods

The main reagents used in this study were MDI, 250 Da and BDO, used as chain extender. For the soft segment chemistry, different PCL diols with molecular weights of 650 (PCL650), 1250 (PCL1250) and 2000 (PCL2000) were selected as polyesters, and poly-(tetramehtyleneoxide) (PTMO2000, 1250 and 650 Da) as polyethers, all being supplied by Sigma–Aldrich.

Sintered HA powder was obtained from Plasma Biotal, Tideswell, UK. The particles were approximately spherical, with an average size of around 3 μm, and were stored in an oven at 60°C until being used. Butylated hydroxyanisole (BHA, from Sigma–Aldrich) was stored at room temperature in a desiccator and protected from visible light.

2.1 Polymer synthesis

All PU's were synthesised in bulk at a NCO/OH ratio of 1.05. A two-step process was adopted. First, a certain amount of PCL diol was kept in a four-neck glass reactor equipped with a stirrer and heated by an oil bath kept at 75°C, under nitrogen atmosphere. The polyol developed into a viscous fluid that was stirred for 24 h, to eliminate any residual moisture. Then, the diisocyanate was added to the polyol and the system was allowed to react for 3 h, yielding a pre-polymer with excess of NCO groups. The final step consisted in extending the pre-polymer by adding BDO, which provided the required OH groups to complete the polymer. Any essential additives (namely BHA) were introduced at this stage. The reaction continued until the increasing viscosity prevented continuation of stirring. The reaction products were kept for 24 h at 60°C under nitrogen. The various molar compositions produced with this method are presented in Table 1. The polymers were cut into pellets of 15 mm^3 approximately and stored in a desiccator protected from light, at room temperature.

2.2 Preparation of the composites

The ceramic filler (HA) and the polymer pellets were premixed manually and then dried for 24 h in an oven at 75°C, to remove any residual moisture. The extrusion of this material was carried out in a prototype mini-extruder, provided with a conventional three-zone Archimedes-type screw with a diameter of 11 mm and a length of 350 mm, rotating at 25 rpm inside a barrel provided with three independently controlled temperature zones (set at 170, 180 and 190°C from hopper to die, respectively). The extruder was coupled to a circular die also kept under controlled temperature, to produce extrudates with a diameter of 2.5 mm. Composites with 30, 50 or 70 wt% of filler were manufactured using the various polymers (and coded as, for example, PU1/30HA, where PU1 refers to the polymer in Table 1 and 30HA identifies the amount of

Table 1 PU compositions

Polymer	Reagents						
	PCL diol (mol)		PTMO diol (mol)		MDI (mol)	BDO (mol)	BHA (% weight)
	2000 Da	1250 Da	2000 Da	650 Da			
PU1	0.017				0.0367	0.018	
PU2		0.017			0.0367	0.018	
PU3			0.017		0.0367	0.018	
PU4			0.017		0.0367	0.018	3
PU5				0.052	0.1090	0.018	0.1

HA). For the sake of homogenization, the composites with 70% filler content were processed in two steps: first, the extruded materials with 50% (m/m) filler were milled, and pre-mixed with ceramic filler to the desired percentage; then, they were submitted to a new extrusion.

2.3 Characterization

PU surfaces were characterized by attenuated total reflectance-Fourier transform infrared spectroscopy (ATR-FTIR) and atomic force microscopy (AFM). ATR-FTIR data was collected at room temperature using a NICOLET 170sx spectrometer. The spectra were obtained with a resolution of 4 cm^{-1} and recorded at a 45° incident angle using a Ge crystal. At least 50 scans were recorded for each sample. The absorbance peak between 1600 and 1800 cm^{-1} (which represents the carbonyl stretching vibration mode of the urethane group) was used as internal reference for intensity comparison. The topography was scrutinized with a Nanoscope III AFM, from Digital Instruments. Surface probing was performed using a 'V-shaped' cantilever with a Si_3 N_4 tip. The surfaces were examined in air, at room temperature (30 × 30 μm^2 areas were scanned in tapping mode; for further detail, areas of 500 × 500 nm^2 were also examined). DSC thermographs were recorded by a Shimadzu DSC 60, after heating samples weighing between 9 and 20 mg from −60 to 250°C, at a rate of 10°C/min. An Indium standard was used for calibration. All samples were re-heated in same conditions in order to eliminate any previous thermal history.

The linear viscoelastic response of the various materials was measured in a Reological Instruments StressTech HR Rotational Rheometer, by performing isothermal frequency sweeps from 10^{-3} to 10^{2} Hz. The tests were carried out at 150°C, using a parallel plate geometry, on discs with a diameter of 2.5 mm and 1 mm thick, obtained by compression moulding at 180°C (applied pressure of 5 MPa during 10 min). Preliminary tests ensured that the deformations imposed were kept within the material linear viscoelastic response. The usual G', G'', tanδ and η^* rheological parameters (elastic modulus, dissipative modulus, loss tangent and dynamic viscosity, respectively) were obtained.

Fractured surfaces of some composites were observed by Scanning Electron Microscopy (SEM) (Hitachi S-4100) in order to assess filler distribution, with an acceleration voltage of 25 kV.

3 Results and discussion

3.1 FTIR spectra of poly(ester urethanes)

Figure 1a compares the infrared spectra of PU1 and PU2. Both polymers exhibit urethane carbonyl stretching vibrations, assigned at 1724 and 1700 cm^{-1}, characteristic of free- and dative-bonded carbonyl groups (C=O), respectively, in the urethane moieties [14]. Dative bonds are established between nitrogen of urethane groups and oxygen of urethane and ester groups (Fig. 2), because the urethane linkage (–NH–CO–O) has a strong proton donor

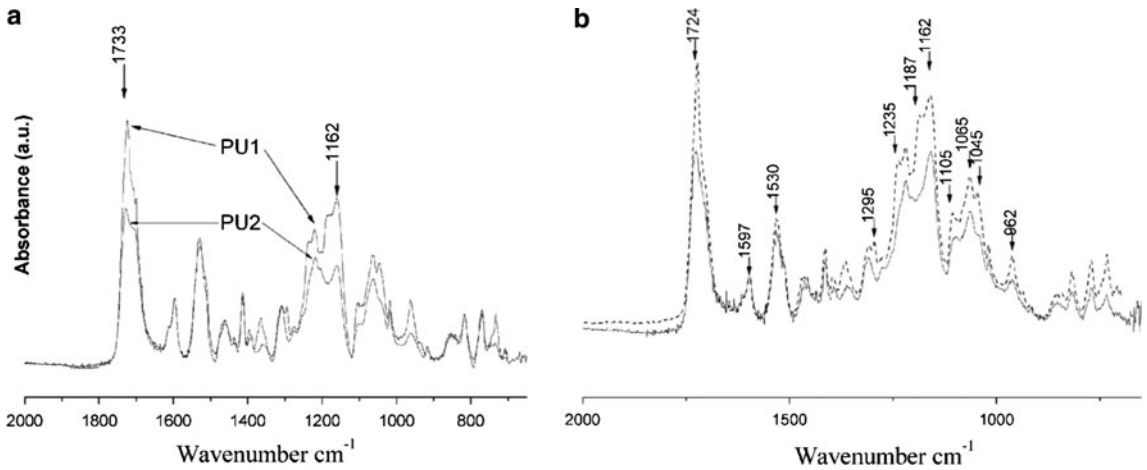

Fig. 1 Ageing effect on IR spectra of PU1 and PU2. **a** PU1 and PU2 65 days after synthesis. **b** PU1 10 days (*solid line*) and 65 days after synthesis (*dashed line*)

Fig. 2 Hydrogen bonding in the polyurethane chain

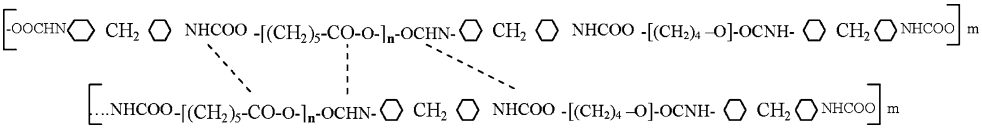

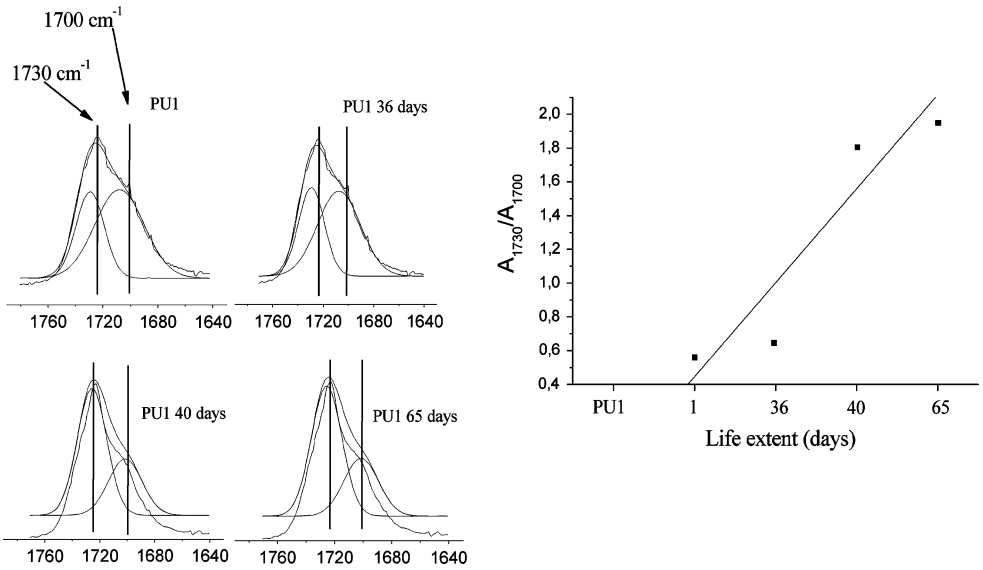

Fig. 3 Influence of ageing on PU1 peak area IR absorption intensity ratio at 1700 cm^{-1} (A_{1700}) vs. 1730 cm^{-1} (A_{1730}). 0 to 65 days after synthesis

group (N–H), and carbonyl groups (C=O) that act as proton receptors [22, 23].

Absorptions at 1530 and 1223 cm^{-1} correspond to amide (NH) in urethane (–NHCOO–) [9]. Absorptions at 1464, 1392 and 1360 cm^{-1} evidence several vibration modes of CH_2 groups. Peaks at 1235, 1162 and 1065 cm^{-1} can be attributed to the stretching vibration of the ester group (–CO–O–) and stretching of the ether group C–O–C is associated with the absorption at 1105 cm^{-1} [23]. Moreover, Fig. 1a shows a higher peak intensity of PU at 1733 cm^{-1} (free C=O), which indicates that increasing PCL chain length decreases the extension of hydrogen bonding, as well as the amount of hard segments [23]. This is coherent with smaller absorption of PU2 at 1162 cm^{-1}, which is indicative of a larger hard segment concentration.

Interestingly, 65 days after PU1 synthesis, the intensity at 1724 cm^{-1} is higher than that for a younger polymer (10 days old), as shown in Fig. 1b. This phenomenon can be attributed to the internal mobility of polymeric chains upon aging, with segregation of soft segments to the surface.

Reduction of the 1700 cm^{-1} band and greater intensities at 1162, 1065 and 1045 cm^{-1} indicate the presence of –CO–O– groups [24], and are a sign that PU's with soft segments based on PCL diol can suffer crystallization changes during storage. This tendency can be confirmed in Fig. 3, where peak areas at 1724 cm^{-1} (A_{1730}) and 1700 cm^{-1} (A_{1700}), obtained by Gaussian deconvolution of PU1 spectra, are related with the shelf life of PU1. Assignments of infrared peaks of the figures discussed above are shown in Table 2.

3.2 FTIR spectra of poly(ether urethanes)

Three poly(ether urethanes) were synthesised (PU3, PU4 and PU5). In PU3 and PU4 the polyol (PTMO) chain length was identical. In the case of PU4, an oxygen radical scavenger (BHA) was added (3% m/m), in order to evaluate the protection effect on biostability. In PU5 the polyol chain length was smaller (650 Da) and only 0.1% (m/m) of BHA was added.

The assignments of the infrared peaks of poly(ether urethanes) PU3 and PU4 are compared in Fig. 4.

No significant differences are observed, probably because the absorption range of the BHA present in PU4 is localized between 1500 and 1000 cm^{-1} (Fig. 5), which coincides with the predominant polymer absorption range. Some absorption bands resembling those observed in poly(ester-urethanes) are also present in the poly(ether-urethanes). Absorptions at 1730 and 1700 cm^{-1} are present. Another absorption band, situated at 1591 cm^{-1}, corresponds to C=C stretching [11]. The C–N and N–H vibrations of the urethane group are identified at 1530 and 1310 cm^{-1}, respectively. The presence of the aromatic ring is detected by the C–C vibration peak at 1413 cm^{-1}, while that at 1017 cm^{-1} is representative of C–H vibration. The ether groups generate the 1110 and 1079 cm^{-1} peaks, corresponding to aliphatic (C–O–C) and urethane (C–O–C=C) ether groups, respectively.

Figure 6 reproduces the IR spectra of PU4 immediately following synthesis and after 36 days. The latter shows a stronger expression of the unbonded carbonyl peak at 1730 cm^{-1}. The same trend is found for other ageing times (Fig. 7). As in polyester urethanes an increase in the area ratio of free to hydrogen-bonded carbonyl (C=O) peaks represents a decrease in hydrogen bonding with storage time.

3.3 Influence of PTMO chain length on FTIR spectra

When comparing isochronal IR spectra of PU3 and PU5 (Fig. 8), the higher intensity of the 1700 cm^{-1} band in the

Table 2 Assignments of the main peaks in the ATR-FTIR spectra of the PU's [25, 26]

PU1		PU2		PU3		PU4		PU5	
W.N. (cm^{-1})	Assignments	W.N. (cm^{-1})	Assignments	W.N. (cm^{-1})	Assignments	W.N. (cm^{-1})	Assignments	W.N. (cm^{-1})	Assignments
1733	ν(C=O) in carbonate free	1737	ν(C=O) in carbonate free	1733	ν(C=O) in carbonate free	1733	ν(C=O) in carbonate free	1730	ν(C=O) in carbonate free
1700	ν(C=O) in carbonate bonded	1705	ν(C=O) in carbonate bonded	1700	ν(C=O) in carbonate bonded	1700	ν(C=O) in carbonate bonded	1700	ν(C=O) in carbonate bonded
1530	δ(N–H) + ν(C–N) in urethane	1533	δ(N–H) + ν(C–N) in urethane	1591	ν(C=C)	1591	ν(C=C)	1589	ν(C=C)
1464	$\delta(CH_2)$	1469	$\delta(CH_2)$	1530	δ(N–H) + ν(C–N) in urethane	1530	δ(N–H) + ν(C–N) in urethane	1527	δ(N–H) + ν(C–N) in urethane
1400	ν(C–C) in benzene ring	1409	ν(C–C) in benzene ring	1413	ν(C–C) in benzene ring	1413	ν(C–C) in benzene ring	1400	ν(C–C) in benzene ring
1235	ν(–CO–O–C–)	1240	ν(–CO–O–C–)	1310	ν(C–N) in urethane + $\omega(CH_2)$	1310	ν(C–N) in urethane + $\omega(CH_2)$		
1223	ν(C–N) in urethane + $\omega(CH_2)$	1223	ν(C–N) in urethane + $\omega(CH_2)$						
1105	ν(C–O–C)	1106	ν(C–O–C)	1110	ν(C–O–C)	1110	ν(C–O–C)	1100	ν(C–O–C)
1065	ν(–CO–O–C–)	1068	ν(–CO–O–C–)	1079	ν(–CO–O–C–)	1079	ν(–CO–O–C–)	1065	ν(–CO–O–C–)

ν stretching vibration, δ bending, ω wagging

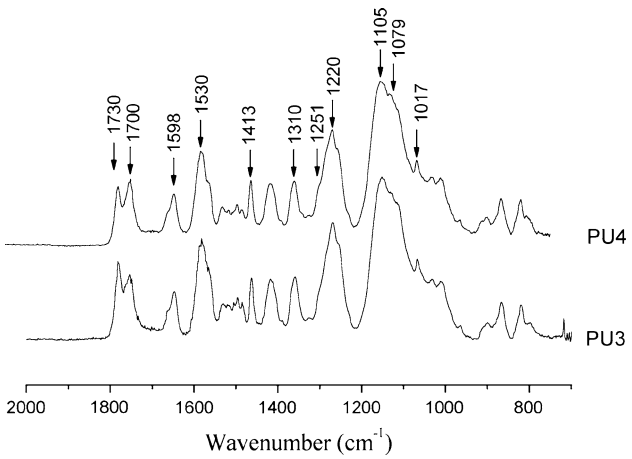

Fig. 4 IR isochronal spectra of PU3 and PU4

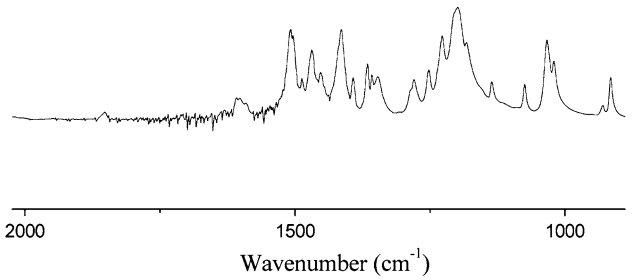

Fig. 5 IR spectra of BHA

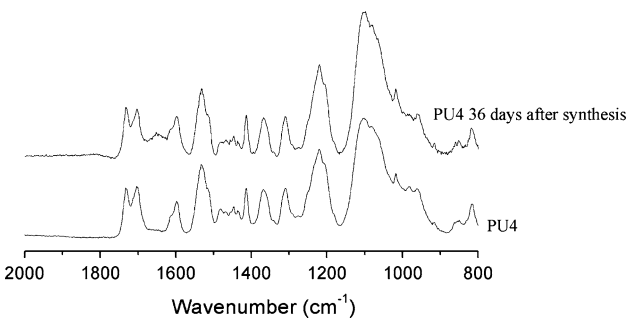

Fig. 6 Ageing effect on PU4 IR spectra, following synthesis and after 36 days

former becomes evident. On the other hand, a higher concentration in hydrogen bonded (C=O) is shown by the expression of the 1700 cm^{-1} peak in PU5, which may be due to a greater concentration of hard segments. As discussed above, other significant bands visible at 1100 and 1079 cm^{-1} are related to the absorption of the ether group (C–O–C). The higher absorption of the 1100 cm^{-1} peak for PU3 is caused by the higher concentration of soft segments. The band at 1079 cm^{-1} (ether in urethane group NC–O–C) is more intense for PU3 thus revealing changes created by

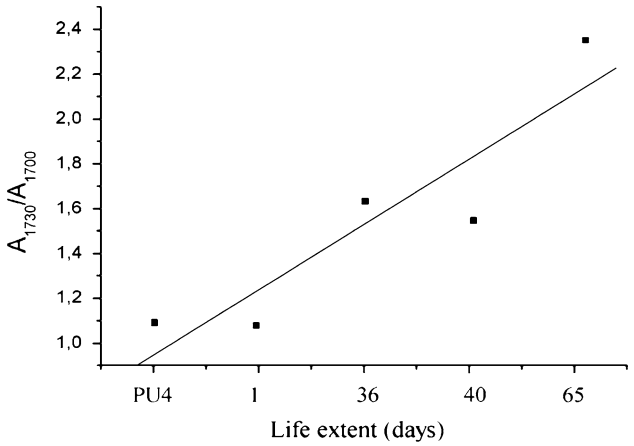

Fig. 7 Dependence of A_{1730}/A_{1700} peak area ratio on ageing time in PU4

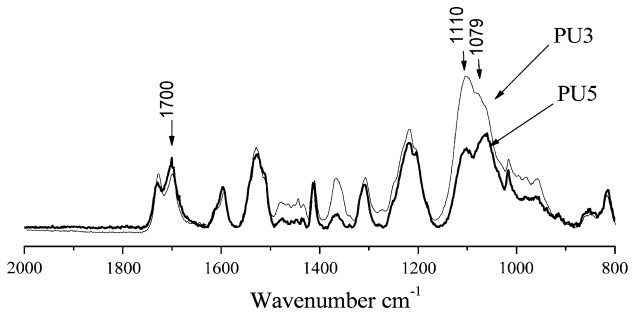

Fig. 8 Influence of PTMO chain length on PU3 and PU5 IR spectra, after 3 days

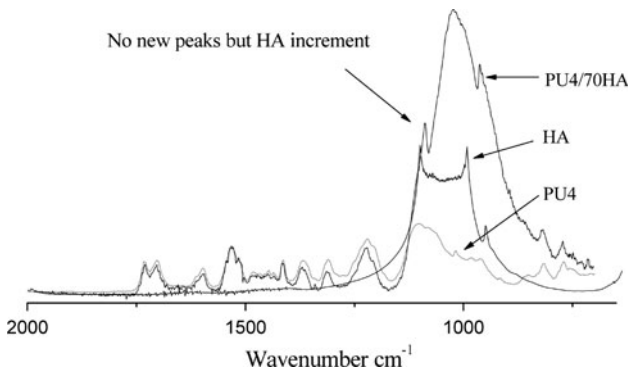

Fig. 9 Effect of addition of HA particles on matrix IR spectra

varying the polyol molecular weight. As the latter decreases, the 1079 to 1100 cm^{-1} ratio increases and so does the hard segment content [27, 28].

Figure 9 shows the effect of the presence of HA particles in the composite (in terms of ATR-FTIR scans of PU4 versus PU4/70HA). Although no new peaks are detected, the composite displays more intense traces from 1200 to 800 cm^{-1}, which result directly from the contribution of the peaks due to HA in this region. Consequently, it seems reasonable to assume that there is no chemical interaction between filler and polymer.

3.4 AFM

In the AFM phase images of PU3 and PU5 (Fig. 10) the brighter zones indicate the presence of hard segments. The area occupied by these in PU3 seems to be smaller than in PU5, which is in agreement with the FTIR data, pointing to the harder character of PU5. The hard phase domain size lies between 25 and 100 nm.

3.5 DSC

DSC traces of PU1 and PU2 are shown in Fig. 11. Two endothermal effects can be observed, one at temperatures within approximately −43 to −19°C, related to the glass transition (T_g), the second in the range of −5 to −1°C, that can be attributed to moisture evolution. The data is listed in Table 3, where the transition temperature T_g is defined as the central point of the transition obtained in the second run (carried out in order to eliminate any previous thermal history [23]). T_g's were identified at −50, −39 and −15°C for PU1, PU2 and PU5, respectively, in order of increasing content of hard segments. The shift to higher temperatures can be directly correlated with the compatibility between phases, indicating better phase-mixing morphology [29, 30]. Transition temperatures in PU3 and PU4 could not be determined due to the absence of an unambiguous effect in the anticipated temperature range.

The thermal transition denoted as T_d is linked to the softening of organized domains that are highly concentrated in hard segments. The remaining materials (PU3; PU4) present undefined peaks in this region, creating some ambiguity in terms of the temperatures associated with that transition.

Melting of soft segments was assigned to T_m. The corresponding transitions are more pronounced and occur at higher temperatures with increasing polyol molecular weight, according to the sequence PU1 > PU2 and PU3 > PU5. This transition is less evident in ether-based PU's, for reasons that are not entirely clear. For example, in the case of PU5 (48% of hard segments) this transition is hardly detected. Phase interactions might be lower compared to similar polyester-based materials, because of the lower potential for hydrogen bonding of ether groups, in comparison with carbonyl (in the ester groups). Such connections will barely exist in hard segment/hard segment interactions, specifically in urethane groups (–NH–CO–O).

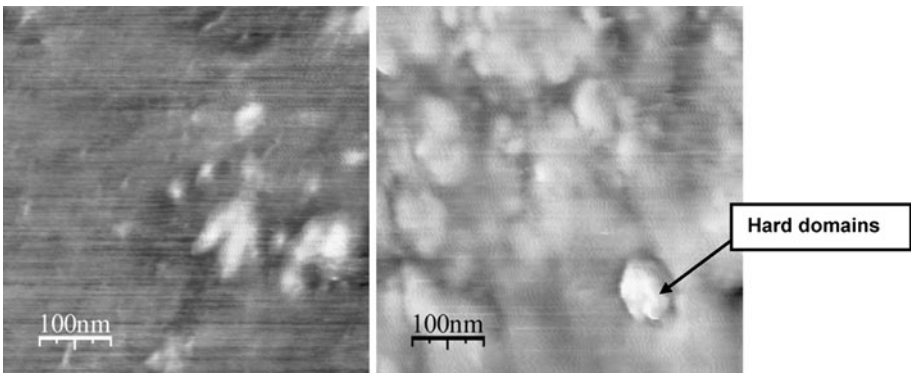

Fig. 10 Influence of PTMO chain length on hard domain concentration. AFM phase images of PU3 (*left*) and PU5 (*right*)

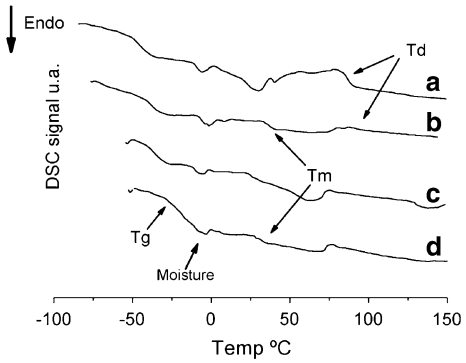

Fig. 11 DSC thermographs of polyurethanes with different polyol chain lenghts: **a** PU1, 1st run, **b** PU1, 2nd run, **c** PU2, 1st run, **d** PU2, 2nd run. Heating rate 10°C/min

Table 3 Thermal properties of PCL and PTMO based polyurethanes

Polyurethane	Hard segm. (%)	First run			Second run		
		T_g (°C)	T_m (°C)	T_{d1} (°C)	T_g (°C)	T_m (°C)	T_d (°C)
PU1 (PCL-2000)	24.13	–41	23	86	–50	34	91
PU2 (PCL-1250)	33.80	–28	25	78	–40	27	79
PU3 (PTMO-2000)	24.13	–	47	–	–58	41	–
PU4 (PTMO-2000)	23.41	–	–	–	–	–	–
PU5 (PTMO-650)	48.48	–15	28	94–147	–15	34	96–140

Tm thermal transition associated to soft segments. *Td* thermal transition associated to hard segments

3.6 Rheology

Figure 12 presents the rheological behaviour of the various polymers in terms of dynamic viscosity, η^* and elastic modulus, G'. As typical of most polymers, these values decrease with increasing frequency, no trace of a Newtonian plateau at the lower frequency range being visible. Viscosity levels are high due to the low test temperature, which was selected in order to avoid material degradation caused by the long residence times in the rheometer.

The relative viscosity/elasticity levels for the various polymers can be easily discriminated, with $\eta^*_{PU3} > \eta^*_{PU1} > \eta^*_{PU5} > \eta^*_{PU4}$ (and the same for G'). The polyether-based polymer (PU3) shows higher complex viscosity than the polyester based polymer with similar chain length (PU1), due to differences in viscosity of the corresponding poliols [31]. Furthermore, viscosity increases with increasing polyol chain length ($\eta^*_{PU3} > \eta^*_{PU5}$) and/or phase-separated morphology, as determined previously by DSC studies. AFM images (Fig. 10) showed that PU5 exhibits a higher area of bright zones than PU3, indicating a lower soft phase content and, consequently, lower values of G'. As discussed above, the presence of free BHA in PU4 produces a plasticization effect, hence a lower viscosity level, due to the differences in chain length and lack of chemical interaction.

Figure 13 presents the same data as Fig. 12, but for the case of the composites reinforced with 30% of HA. The relative ranking of the materials remains generally the same. For the case of PU1 (Fig. 13), addition of HA causes a decrease in complex viscosity especially in the low frequency range, and a more important increase in elasticity. This is surprising and contrary to the anticipated behaviour. However, it is well known that suspensions may exhibit anomalous rheological behaviour, which has been attributed to the occurrence of a number of (individual or combined) effects such as wall-slip [32, 33], rotation of the filler particles (Mooney and Wolstenholme [34] proposed a model of "supermolecular flow" involving the rotation of particles or groups of molecules as elastic bodies), or local lubrication (flow of the matrix between adjacent filler particles develops high local shear rates, hence viscosity decreases) [35]. These effects should be higher if matrix-particle interaction is small, which is the case as discussed above (see Fig. 9). Therefore, as the (–OH) groups of HA react with free isocyanate, a strong interaction between HA and PU would induce an increase in viscosity. Since the

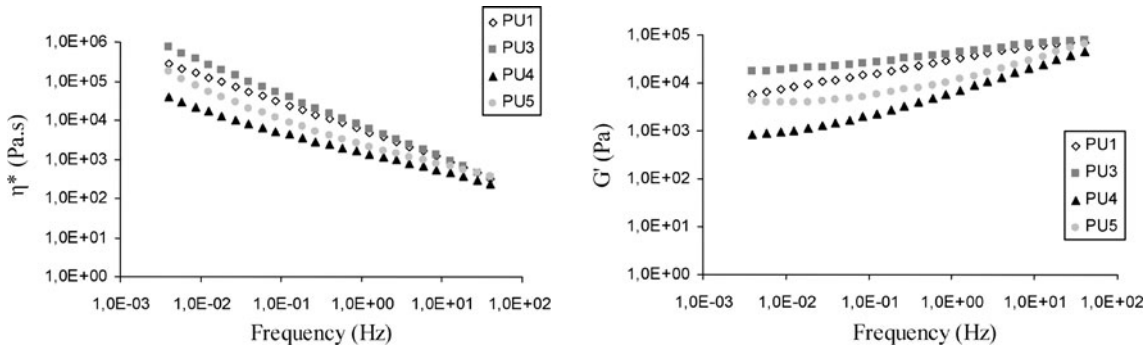

Fig. 12 Dynamic viscosity (η^*) and storage modulus (G') for the unfilled polymers

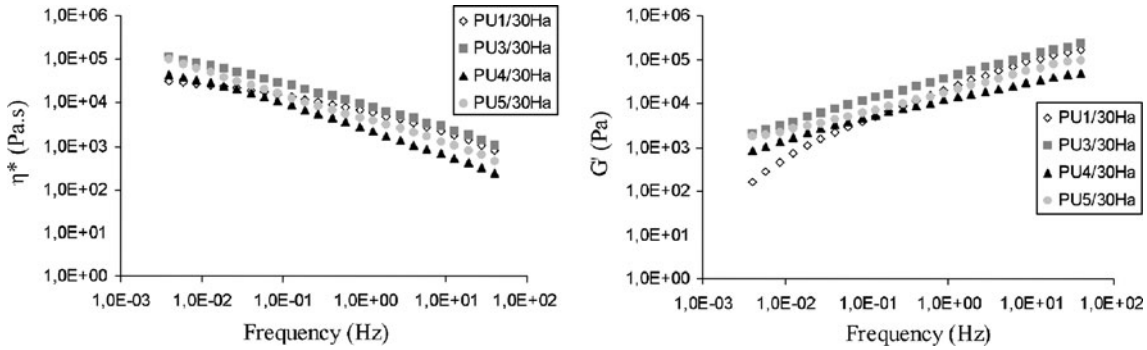

Fig. 13 Dynamic viscosity (η^*) and storage modulus (G') for the PU-HA composites with 30% HA

opposite was observed (Fig. 13), one can therefore assume that practically all isocyanate has reacted.

Although no systematic rheological characterization of PU-HA composites seems to have been reported in the literature, interfacial stick–slip transition was reported for PE-HA composites, even at low incorporation content, during flow in a capillary rheometer [36]. Since the data presented in Fig. 14 was obtained from oscillatory tests on PU1 and PU5 polymers and composites, one would deduce that wall-slip effects would prevail. A second, eventually complementary cause for this rheological behaviour could be presence of a relatively poorly mixed composite. It is well known that single screw extruders provide good distributive mixing but cannot achieve high dispersion levels, the prototype mini-extruder used in this study being no exception. As an example, Fig. 15a, b, shows a homogeneous composite (PU5) with high filler content (70%), where the ceramic particles are relatively well dispersed in the matrix, while Fig. 15c reveals that other materials (e.g., PU1), with lower mineral content (30%), may show HA agglomeration.

Raising the degree of incorporation from 30 to 50% does not seem to affect the viscoelastic behaviour of the composite; however, when the filler concentration is further increased to 70% the rheological response changes dramatically (see Fig. 14), a solid-like behaviour with high values of η^* and G' being evident. McGeary [37] showed experimentally that the close packing of particles of uniform size corresponds to a maximum density between 60 and 64% (body centered cubic or hexagonal close packing). In other words, as the percentage of HA increases, the suspension with a relative highly concentration of solids is progressively converted into an association of solid particles with liquid deposited in interstices and a thin film surrounding their surface.

4 Conclusions

PU/HA composites with different matrix chemistries were prepared by extrusion, following a methodology that can be easily scaled-up to industrial production.

Various PU's were obtained from polyester and poly(-ether-urethanes), and characterized in some detail, revealing the presence of different hard segment contents, probably related to different concentrations of hydrogen bonds between urethane linkages.

As the polyol chain length decreases, the 1079 to 1100 cm^{-1} ratio increases and so does the hard segment content.

PU's with soft segments based either on PCL diol or on polyol can suffer crystallization changes during ageing,

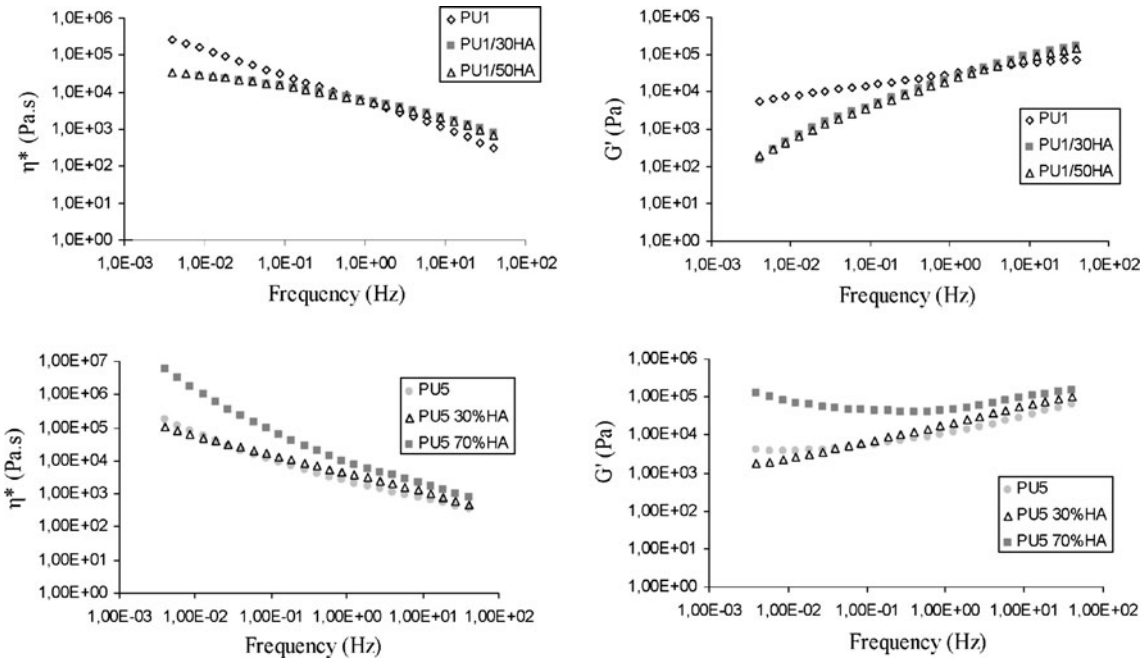

Fig. 14 Effect of filler content on dynamic viscosities (η^*) and storage moduli (G'). PU1 (0; 30 and 50% HA) and PU5 (0; 30 e 70% HA)

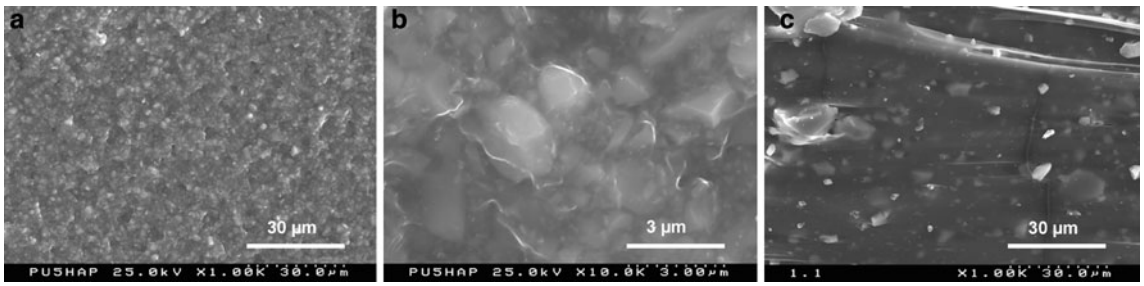

Fig. 15 Fractographic view of samples with different filler content: **a** PU5/70HA, **b** PU5/70HA, **c** PU1/30HA

with a reduction in the concentration of dative bonds and possible segregation of soft segments to the surface.

Rheological studies revealed that the presence of free BHA, PU4, produces a lower viscosity level, due to the differences in chain length and lack of chemical interaction.

The processability of the polymers enabled the preparation of composites with high filler content and relatively good homogeneity. However, the HA particles were not fully wetted by the matrix at higher filler contents.

Future investigations with these materials will involve studying their chemical stability, and evaluating their mechanical performance and biocompatibility in vitro. Eventually, the chemical bonding of HA to the matrix will possibly require some improvement.

Acknowledgments The authors would like to acknowledge the financial support of Centre for Research in Ceramics and Composite Materials research project CTS 2002-05.

References

1. Liu Q, de Wijn JR, van Blitterswijk CA. A study on the grafting reaction of isocyanates with hydroxyapatite particles. J Biomed Mater Res. 1998;40:358–64.
2. That PT, Tanner KE, Bonfield W. Fatigue characterization of a hydroxyapatite-reinforced polyethylene composite. I. Uniaxial fatigue. J Biomed Mater Res. 2000;51:453–60.
3. Di Silvio L, Dalby MJ, Bonfield W. Osteoblast behaviour on HA/PE composite surfaces with different HA volumes. Biomaterials. 2002;23:101–7.
4. Dalby MJ, Bonfield W, Di Silvio L. Enhanced HAPEX topography: comparison of osteoblast response to established cement. J Mater Sci Mater Med. 2003;14:693–7.
5. Ladizesky NH, Ward IM, Bonfield W. Hydrostatic extrusion of polyethylene filled with hydroxyapatite. Polym Adv Technol. 1997;8:496–504.
6. Wang M, Hench LL, Bonfield W. Bioglass/hight density polyethylene composite for soft tissue applications: preparation and evaluation. J Biomed Mater Res. 1998;42:577–86.
7. Matheson LA, Labow RS, Santerre JP. Biodegradation of polycarbonate-based polyurethanes by the human monocyte-derived

macrophage and U937 cell systems. J Biomed Mater Res. 2002;61:505–13.
8. Guan J, Sacks MS, Beckman EJ, Wagner WR. Synthesis, characterization, and cytocompatibility of elastomeric, biodegradable poly(ester-urethane)ureas based on poly(caprolactone) and putrescine. J Biomed Mater Res. 2002;61:493–503.
9. Pinto UA, Visconte LLY, Nunes RCR. Mechanical properties of thermoplastic polyurethane elastomers with mica and aluminium trihydrate. Eur Polym J. 2001;37:1935–7.
10. Finnigan B, Martin D, Halley P, Truss R, Campbell K. Morphology and properties of thermoplastic polyurethane nanocomposites incorporating hydrophilic layered silicates. Polymer. 2004;45:2249–60.
11. Farè S, Valtulina V, Petrini P, Alessandrini E, Pietrocola G, Tanzi MC, Speziale P, Visai L. In vitro interaction of human fibroblasts and platelets with a shape memory polyurethane. J Biomed Mater Res. 2005;73A:1–11.
12. Christenson EM, Anderson JM, Hiltner A. Oxidative mechanisms of poly(carbonate urethane) and poly(ether urethane) biodegradation: in vivo and in vitro correlations. J Biomed Mater Res. 2004;70A:245–55.
13. Veleva AN, Khan SA, Cooper SL. Oxidative and hydrolytic stability of a novel acrylic thermopolymer for biomedical applications. J Biomed Mater Res. 2005;74A:117–23.
14. Schubert MA, Wiggins MJ, Anderson JM, Hiltner A. Role of oxygen in biodegradation of poly(etherurethaneurea) elastomers. J Biomed Mater Res. 1997;34:519–30.
15. Roeder RK, Sproul MM, Turner CH. Hydrpxyapatie whiskers provide improved mechanical properties in reinforced polymer composites. J Biomed Mater Res. 2003;67A:801–12.
16. Yu R, Tan TH, Kong AN. Butylated hydroxyanisole and its metabolite tert-butylhydroquinone differentially regulate mitogen-activated protein kinases. The role of oxidative stress in the activation of mitogen-activated protein kinases by phenolic antioxidants. J Biol Chem. 1997;272:28962–70.
17. Yu R, Mandlekar S, Kong AN. Molecular mechanisms of butylated hydroxylanisole-induced toxicity: induction of apoptosis through direct release of cytochrome c. Mol Pharmacol. 2000;58:431–7.
18. US. Food and Drug Administration (2006).
19. Kalus WH , Münzner R, Filby WG. The reaction of butylated hydroxyanisole and its metabolites with some arylamines: investigations of product mutagenicity. Environ Health Persp. 1994;102:1.
20. Kahl R. Synthetic antioxidants: biochemical actions and interference with radiation, toxic compounds, chemical mutagens and chemical carcinogens. Toxicology 1984;33:185–228.
21. Kahl R, Weinke S, Kappus H. Production of reactive oxygen species due to metabolic activation of butylated hydroxyanisole. Toxicology (1989);59:179–94.
22. Szycher M. Szycher's handbook of polyurethanes. New York, Washington: CRC Press; 1999.
23. Gorna K, Gogolewski S. Synthesis and characterization of biodegradable poly(-caprolactone urethane)s. I. Effect of the polyol molecular weight, catalyst, and chain extender on the molecular and physical characteristics. J Polym Sci A Polym Chem. 2002;40:156–70.
24. Gorna K, Gogolewski S. Biodegradable polyurethanes for implants. II. In vitro degradation and calcification of materials from poly(ε-caprolactone)-poly(ethylene oxide) diols and various chain extenders. J Biomed Mater Res. 2002;60:592–606.
25. Srichatrapimuk VW, Cooper SL. Infrared thermal analysis of polyurethane block polymers. J Macromol Sci B Phys. 1978;15:267–311.
26. Bellamy LJ. The infrared spectra of complex molecules. London: Chapman and Hall; 1975.
27. Khan I, Smith N, Jones E, Finch DS, Cameron RE. Analysis and evaluation of a biomedical polycarbonate urethane tested in an in vitro study and an ovine arthoplasty model. Part I: materials selection and evaluation. Biomaterials. 2005;26:621–31.
28. Ho SP, Nakabayashi N, Iwasaki Y, Boland T, LaBerge M. Frictional properties of poly(MPC-co-BMA) phospholipid polymer for catheter applications. Biomaterials. 2003;24:5121–9.
29. Chen H, Jiang X, He L, Zhang T, Xu M, Yu X. Novel biocompatible waterborne polyurethane using L-Lysine as an extender. J Appl Polym Sci. 2002;84:2474–80.
30. Skarja GA, Woodhouse KA. Structure-property relationships of degradable polyurethane elastomers containing an amino acid-based chain extender. J Appl Polym Sci. 2000;75:1522–34.
31. Macosko C. Rheology—principles, measurements and applications. New York: Wiley-VCH; 1994.
32. Chryss AG, Bhattacharya SN, Pullum L. Rheology of shear thickening suspensions and the effects of wall slip in torsional flow. Rheol Acta. 2005;45:124.
33. Denn MM. Extrusion instabilities and wall slip. Annu Rev Fluid Mech. 2001;33:265.
34. Mooney M, Wolstenholme WE. The rheological unit in raw elastomers. J Appl Phys. 1954;25:1098.
35. Bernardo CA, Van Hattum FWJ, Carneiro OS, Maia JM. The role of rheology in the processing of vapor grown carbon fiber/thermoplastic composites, NATO ASI series: carbon filaments and nanotubes: common origins, differing applications. Dordrecht: Kluwer Academic Publishers; 2001. p. 289.
36. Joseph R, Martyn MT, Tanner KE, Coates PD. Interfacial stick-slip transition in hydroxyapatite filled high density polyethylene composite. Bull Mater Sci. 2006;29:85–9.
37. McGeary K. Mechanical packing of spherical particles. J Am Ceram Soc. 1961;44:513–22.